Collinear optical coherence and confocal fluorescence microscopies for tissue engineering

J. P. Dunkers, M. T. Cicerone and N. R. Washburn

Polymers Division, National Institute of Standards and Technology
100 Bureau Dr., Stop 8541, Gaithersburg, MD 20899
joy.dunkers@nist.gov

Abstract: Tissue engineered medical products (TEMPs) are often three-dimensional (3D) hybrid materials consisting of a porous scaffold upon which the tissue is grown. However, monitoring of the developing tissue deep within the scaffold is hampered by its turbidity. We have sought new ways to probe the interior of the scaffold with the same resolution as conventional laser scanning confocal microscopy but with greater sensitivity. We present a novel application of optical coherence microscopy (OCM) by combining it with confocal fluorescence microscopy (CFM) to gather simultaneous structural and functional information on TEMPs in a registered fashion. In this work, we describe the collinear OCM and CFM instrument. We demonstrate the utility of this dual-mode technique for TEMPs by imaging fluorescently stained osteoblasts cultured in a polymeric TEMP.

OCIS codes: (170.0180) Microscopy; (180.6900) Three-dimensional microscopy; (170.0110) Imaging systems; (170.1650) Coherence imaging; (170.2520) Fluorescence microscopy

---

References and links

1. J. M. Anderson, L. G. Cima, S. G. Eskin, et al., "Tissue engineering in cardiovascular disease - a report," J. Biomed. Mater. Res. **29**, 1473-1476 (1995).
2. J. Izatt, M. Kulkarni, H.-S. Wang, K. Kobayashi, and M. Sivak, "Optical coherence tomography and microscopy in gastrointestinal tissues," IEEE J. Sel. Top. Quantum Electron. **2**, 1017-1028 (1996).
3. S. Chinn and E. Swanson, "Blindness limitations in optical coherence domain reflectometry," Electron. Lett. **29**, 2025-2027 (1993).
4. F. Thorsen, T.-A. Read, M. Lund-Johansen, B. B. Tysnes, and R. Bjerkvig, "Alginate-encapsulated producer cells: a potential new approach for the treatment of malignant brain tumors," Cell Transplantation. **9**, 773-783 (2000).
5. M. Attawia, J. Devin, and C. Laurencin, "Immunofluorescence and confocal laser-scanning microscopy studies of osteoblast growth and phenotypic-expression in 3-dimensional degradable synthetic matrices," J. Biomed. Mat. Res. **29**, 843-848 (1995).
6. M. Afting, U. Stock, B. Nasseri, I. Pomerantseva, B. Seed, and J. Vacanti, "Efficient and stable retroviral transfection of ovine endothelial cells with green fluorescent protein for cardiovascular tissue engineering," Tissue Eng. **9**, 137-41 (2003).
7. F. Guzman and J. K. Barton, "Dual OCT/spectroscopy system for identification of vascular pathology," Proc. SPIE Int. Soc. Opt. Eng. **4244**, 413 –414 (2001).
8. E. Beaurepaire, L. Moreaux, F. Amblard and J. Mertz, "Combined scanning optical coherence and two-photon-excited fluorescence microscopy," Opt. Lett. **24**, 969-971 (2000).
9. S. Demos, M. Staggs, K. Minoshima, and J. Fujimoto, "Characterization of laser induced damage sites in optical components," Opt. Express **10**, 1444-1450 (2002).
   http://www.opticsexpress.org/abstract.cfm?URI=OPEX-10-25-1444
10. Identification of a commercial product is made only to facilitate experimental reproducibility and to adequately describe experimental procedure. In no case does it imply endorsement by NIST or imply that it is necessarily the best product for the experimental procedure.
11. All uncertainties expressed in accordance to: B. Taylor and C. Kuyatt, NIST Technical Note 1297, 1994 and are based on one standard deviation.
12. G. Tearney, M. Brezinski, J. Southern, B. Bouma, M. Hee, and J. Fujimoto, "Determination of the refractive-index of highly scattering human tissue by optical coherence tomography," Opt. Lett. **20**, 2258-2260 (1995).

13. J. O. Iroh, "Poly(ε-caprolactone)" in *Polymer Data Handbook*, J. E. Mark, ed. (Oxford University Press, New York. 1999).
14. N. Washburn, C. Simon, A. Tona, H. Elgendy, A. Karim, and E. Amis, "Co-extrusion of biocompatible polymers for scaffolds with co-continuous morphology," J. Biomed. Mat. Res. **60**, 20-29 (2002).
15. http://www.olympusmicro.com/primer/techniques/fluorescence/fluorotable2.html

1. Introduction

Tissue engineering is an emerging interdisciplinary field that "creates devices for the study, restoration, modification and assembly of functional tissues from native or synthetic sources" [1]. Tissue engineered medical products (TEMPs) often consist of a three-dimensional synthetic scaffold that provides form and foundation for the cells as they produce the tissue of interest. Successful TEMPs will allow cell infiltration and foster proliferation and differentiation within the scaffold. Cell infiltration and behavior may depend on a multitude of factors intrinsic to the scaffold, including global and local structure, surface composition, and other physical properties, such as modulus. While it is generally understood that a complex interaction of many variables influences the success of the TEMPs, the precise nature of these interactions has yet to be worked out in many instances. A significant difficulty in furthering the understanding of the interaction between these factors and cell behavior is the lack of a high-resolution imaging technique that can penetrate deeply and non-destructively into the scaffold. Towards meeting this need, we have built a collinear optical coherence and confocal fluorescence microscope to non-invasively monitor both structure and function in a TEMP.

Reflection confocal microscopy has been routinely used to reveal details of cells, tissues, and their growth. However, its Lorentzian axial point spread function (PSF) results in a finite collection efficiency even far out of the focus plane, and this limits its use in highly scattering media such as TEMPs [2]. Cellular-level details are also obtained with optical coherence microscopy (OCM), but OCM has the attractive feature of providing extremely good rejection of light scattered out of the focal plane [3]. OCM is an interferometric technique that uses both confocal and coherence gating mechanisms for stray light rejection. Thus, the PSF of OCM drops off in a Gaussian manner far from the focal plane and much more rapidly than that of confocal microscopy [2]. Another advantage of OCM is its dynamic range; > 100 dB is not uncommon, so that even reflection signals that have been attenuated by five orders of magnitude due to scattering can be detected. In this work, we use confocal fluorescence microscopy (CFM) in tandem with OCM for characterizing the cell / scaffold system. CFM suffers from the same relatively poor background rejection as reflection confocal microscopy. However, the added spectral discrimination can significantly extend the depth-of-view for the technique, provided that the background fluorescence is minimal, and that the fluorescent features of interest are limited to discrete, well separated regions. CFM has proven to be an extremely powerful technique for understanding cell viability [4], differentiation [5], and protein expression [6] in tissue engineering. This technique can give functional information to complement the structural information obtained with OCM.

At least two authors have previously used coherence and fluorescence detection methods for acquisition of registered images. Guzman and Barton [7] utilized optical coherence tomography (OCT) and laser induced fluorescence to image ex-vivo canine aorta for the study of arteriosclerosis. Beaurepaire *et al.* [8] used OCM and two-photon fluorescence to image live drosophila embryos. Recently, another paper has recognized the potential impact of OCT in materials science. Researchers used OCT and fluorescence as separate techniques to characterize laser induced defects in optics [9]. In this work we demonstrate collinear OCM and CFM on a semi-crystalline poly(ε-caprolactone) tissue scaffold, and show how these two techniques are synergistic when applied to biological samples embedded in highly scattering media.

2. Experimental

Figure 1 shows a schematic of the OCM/CFM system. The OCM system consists of a broadband, 70 nm FWHM (full width at half maximum), semiconductor optical amplifier-based near infrared (NIR) source (AFC, Hull, Quebec, Canada) [10] centered at 1.31 µm with a maximum output of 10 mW. The detection system is a polarization-maintaining, polarization-sensitive fiber-optic coherence domain reflectometer built by Optiphase (Van Nuys, CA) with a core fiber diameter of 6.6 µm. In this work, we monitor vertical or s polarization only. In the sample arm, the NIR light from a single mode, polarization-maintaining fiber is launched into a bulk optic system via a 0.55 NA collimating lens. The remainder of the optical train for the OCM component consists of a variable neutral density filter, a cold mirror, a 3:1 expanding telescope, and a 1.3 NA Epiplan-Neofluar oil-immersion objective (Zeiss, Germany). Reflected light is returned to the single mode fiber, which acts as a confocal aperture for the detection system. The reference arm of the interferometer is driven by piezoelectric modulators at 300 Hz and filtered at a Doppler frequency of 705 kHz. The sensitivity of the system is 95 dB.

The CFM instrument (Fig. 1) is comprised of an air-cooled Omnichrome argon ion laser (Melles Griot, Carlsbad, CA) at 488 nm. The laser light is chopped at 1.5 kHz, and then sent through a bandpass filter and a dichroic beam splitter before reaching the cold mirror where it is combined with the NIR beam. Because we use a refractive objective, the focal points of the 488 nm and NIR beams are separated by (5.8 ± 0.1) µm [11], with the visible light focused closer to the objective. This effect is accounted for during the image registration process by in upward shift of the OCM images. The fluorescence signal propagates back through the cold mirror to the dichroic beam splitter where the excitation line is filtered out. Confocal gating of the fluorescence signal is accomplished in the usual way by focusing the collected light through long pass filter (>500 nm) and then through a 10 µm pinhole. The fluorescence signal was detected using a photo-multiplier tube (Oriel, Stratford, CT) and lock-in amplifier (Perkin Elmer, Freemont, CA). The axial PSF for detection of the reflected 488 nm light with a 1.3 NA oil immersion lens has a FWHM of (0.58 ± 0.02) µm, which corresponds to a detection pinhole of 0.3 Airy units (AU). The axial resolution of the OCM channel with this objective in place is (1.5 ± 0.3) µm, and is consistent with the theoretical prediction for a detection pinhole of 1 AU. Lateral resolution is expected to be 0.16 µm and 0.51 µm, respectively, for the CFM and OCM channels.

Imaging is performed simultaneously for the OCM and CFM channels. Repeating a process of scanning the sample in the x direction and subsequently stepping in y allows us to create two-dimensional images with a pixelation rate of 300 Hz. The scanning and stepping are accomplished using motorized stages (Newport, Irvine, CA). Stepping in the z direction after each x-y scan is accomplished by a motorized z-axis stage (ASI Inc., Eugene, Oregon). The x-y stages are designed for 5 µm repeatability, and this represents the practical limit on the resolution of our images in this report.
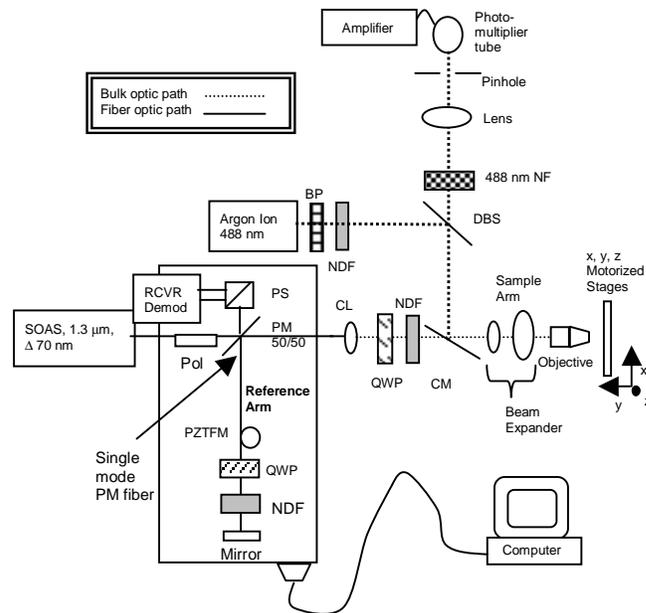
Fig. 1. Experimental apparatus for collinear OCM/ CFM. BP: band pass filter; CL: collimating lens; CM: cold mirror; Demod: Demodulator; SOAS: semiconductor optical amplifier source; DBS: dichroic beam splitter; LP: Long pass filter; NDF: Neutral density filter; NF: Notch filter; PM: Polarization maintaining 50/50 coupler; Pol: In-line polarizer; PS: Polarization splitter; PZTFM: Piezoelectic fiber

3. Results and discussion

The image slices shown in Fig. 2 are of a cultured poly(ε-caprolactone) (PCL) scaffold at a depth of (145 ± 1) μm below the surface, and were obtained with the OCM (A.) and CFM (B.) channels of the instrument described here. The images in Figs. 2 and 4 are 500 μm wide and 1.0 mm high. The image depth was calculated by scaling the distance moved by the stage by the refractive index (n_D) of the sample, (1.50 ± 0.02). The average refractive index of the sample was measured using procedures in the paper by Bouma *et al*. [12]. The scaffold was comprised of semi-crystalline PCL which had 0.50 mass fraction porosity and >65 % crystallinity [13]. A representative scanning electronic micrograph of the uncultured scaffold is shown in Fig. 3 for comparison. Details about the scaffold fabrication process can be found elsewhere [14]. The PCL scaffold was cultured with fetal chick osteoblasts for 10 weeks, stained with nuclear fast red [15], and bathed in a standard refractive index fluid (SPI Supplies, n_D = 1.526) for imaging. The areas of pore and scaffold are designated by the arrows in the OCM channel and have corresponding assignments in the CFM channel. The granularity exhibited in the scaffold itself is derived from the polymeric crystallites. We also see signal in the OCM channel from cells and mineralized matrix deposited by the cells. In principle, the signal in the CFM channel comes exclusively from fluorescence emitted by the nuclear dye, which intercalates deoxyribonucleaic acid, and is concentrated in the cellular nucleus. The red asterisks illustrate several examples where cells appear to line the pore walls in the OCM channel, and have corresponding features in the CFM channel.
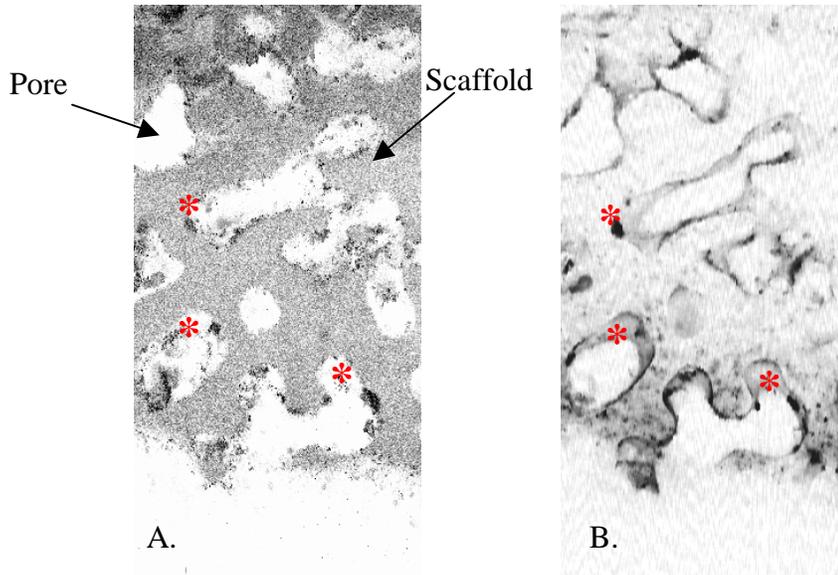
Fig. 2. OCM (A.) and CFM (B.) images 145 μm from surface of PCL cultured for 10 weeks with fetal chick osteoblasts.
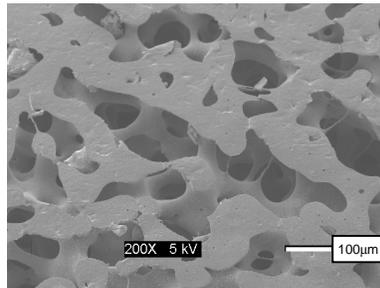
Fig. 3. Scanning electron micrograph of PCL scaffold. PCL was co-extruded with poly-ethyleneoxide (PEO) at 0.50 mass fraction. The scaffold was immersed in solvent to dissolve the PEO, and the remaining PCL was subject to a 30 min anneal at 75 °C.

Figure 4 displays a movie of merged and registered OCM and CFM images of the cultured PCL scaffold that begins at the surface of the scaffold and moves through its thickness. Because of the chromatic aberration issue discussed previously, the images were registered by matching the CFM images with the previous OCM image in the series. The image series spans (330 ± 1) μm. In this movie, regions of no OCM signal are red, high OCM signal are black, and regions of high CFM signal are yellow. Note that the sample is slightly tilted. The OCM and CFM responses from the top of the image are seen before the bottom. Likewise, the fluorescence response at the top of the image fades before the bottom. As the first few slices are viewed, it is evident that cells are present on the surface of the scaffold as

well as lining the pore walls. As expected, the OCM signal has greater sensitivity than the fluorescence as we penetrate deeper into the scaffold. Even as the fluorescence signal fades, the presence of cells lining the pore walls can be seen using OCM as areas of higher reflectivity.

We have sought to enhance the suite of characterization techniques currently used for TEMPs by developing a non-destructive, high-resolution dual mode technique for *in situ* imaging. We have built and characterized a confocal microscope designed to probe both structural and functional aspects of TEMPs through optical coherence and confocal fluorescence microcopies. As a proof of principle, we have demonstrated the use of a combined OCM / CFM for imaging tissues and cells in TEMPs. We have shown that by using these complimentary imaging modalities, we can detect the presence of biological tissues growing deep within the TEMP. CFM compliments OCM by allowing us to positively identify stained tissues at more shallow depths. Once identified, OCM allows us to discriminate these tissues from matrix and scaffold, and thus view them at a greater depth. This approach will form the basis of structure-property relationships for TEMPs based on microscopic characterization of scaffold properties and concomitant cellular responses.
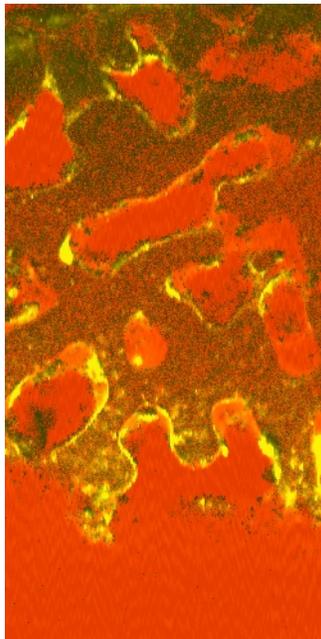
Fig. 4. (0.72 MB) Movie of merged and registered OCM and CFM images of the cultured PCL scaffold.

Acknowledgments